

SurfaceVibe: Vibration-Based Tap & Swipe Tracking on Ubiquitous Surfaces

Shijia Pan

Ceferino Gabriel Ramirez
Carnegie Mellon University
Electrical and Computer Engineering
Moffett Field, California 94086
{shijiapan,cgrramirez}@cmu.edu

John Paul Shen

Carnegie Mellon University
Electrical and Computer Engineering
Moffett Field, California 94086
jpshen@cmu.edu

Mostafa Mirshekari

Jonathon Fagert
Carnegie Mellon University
Civil and Environmental Engineering
Pittsburgh, Pennsylvania 15213
{mmirshekari,jfagert}@cmu.edu

Hae Young Noh

Carnegie Mellon University
Civil and Environmental Engineering
Pittsburgh, Pennsylvania 15213
noh@cmu.edu

Albert Jin Chung

Chih Chi Hu
Carnegie Mellon University
Electrical and Computer Engineering
Moffett Field, California 94086
{albertjc,chihhu}@cmu.edu

Pei Zhang

Carnegie Mellon University
Electrical and Computer Engineering
Moffett Field, California 94086
peizhang@cmu.edu

ABSTRACT

Touch surfaces are intuitive interfaces for computing devices. Most of the traditional touch interfaces (vision, IR, capacitive, etc.) have mounting requirements, resulting in specialized touch surfaces limited by their size, cost, and mobility. More recent work has shown that vibration-based touch sensing techniques can localize taps/knocks, which provides a low-cost flexible alternative. These surfaces are envisioned as intuitive inputs for applications such as interactive meeting tables, smart kitchen appliance control, etc. However, due to dispersive and reflective properties of various vibrating mediums, it is difficult to localize taps accurately on ubiquitous surfaces. Furthermore, no work has been done on tracking continuous swipe interactions through vibration sensing.

In this paper, we present SurfaceVibe, a vibration-based interaction tracking system for multiple surface types. The system accounts for physics properties of different waves to allow two major interaction types: tap and swipe. For tap induced impulse-like surface waves, we design an algorithm that takes wave dispersion and reflection into account to achieve accurate localization on ubiquitous surfaces. For swipe induced body waves, SurfaceVibe segments signals into ‘slip pulses’ to localize, and then tracks the trajectory. We validate SurfaceVibe through experiments on different materials and varying surface/sensing area sizes in this paper. Our methods achieve up to 6X decrease in localization error for taps and 3X reduction in length estimation error for swipes compared to existing algorithms that do not take wave properties into account.

CCS CONCEPTS

•Human-centered computing → *Ubiquitous and mobile computing systems and tools;*

Permission to make digital or hard copies of all or part of this work for personal or classroom use is granted without fee provided that copies are not made or distributed for profit or commercial advantage and that copies bear this notice and the full citation on the first page. Copyrights for components of this work owned by others than ACM must be honored. Abstracting with credit is permitted. To copy otherwise, or republish, to post on servers or to redistribute to lists, requires prior specific permission and/or a fee. Request permissions from permissions@acm.org.

IPSN 2017, Pittsburgh, PA USA

© 2017 ACM. 978-1-4503-4890-4/17/04...\$15.00
DOI: <http://dx.doi.org/10.1145/3055031.3055077>

KEYWORDS

Interaction tracking, surface vibration, wave propagation, dispersion

ACM Reference format:

Shijia Pan, Ceferino Gabriel Ramirez, Mostafa Mirshekari, Jonathon Fagert, Albert Jin Chung, Chih Chi Hu, John Paul Shen, Hae Young Noh, and Pei Zhang. 2017. SurfaceVibe: Vibration-Based Tap & Swipe Tracking on Ubiquitous Surfaces. In *Proceedings of The 16th ACM/IEEE International Conference on Information Processing in Sensor Networks, Pittsburgh, PA USA, April 2017 (IPSN 2017)*, 12 pages.
DOI: <http://dx.doi.org/10.1145/3055031.3055077>

1 INTRODUCTION

Ubiquitous human-machine interfaces have become an integral part of everyday life providing intuitive control input to a wide range of computing devices. In the past decade in particular, touch sensitive surfaces have created an interaction model that is natural and intuitive for users [28]. Presently, many personal devices (e.g. mobile phones and laptops) incorporate touch screens to take advantage of point tracking and gesture recognition to enhance user experience and interaction.

One of the biggest challenges for touch devices is that the interaction area on the device is limited by the device size [3]. Touch input surfaces today are built into the limited device sizes that support them and the cost of designing and manufacturing large, interactive surfaces is high. On the other hand, people reside in places with large physical surfaces. Tabletops and wall surfaces are readily available and are familiar surfaces in people’s lives. These everyday surfaces can potentially be transformed into touch-enabled surfaces. A touch-enabled kitchen tabletop can provide intuitive input to various smart appliances. A touch-enabled meeting table allows participants to join the interaction freely.

Several approaches have been explored to enable input detection on these types of surfaces. Vision-based methods allow gesture tracking and recognition through strategically placed cameras [15, 16, 29]. The vision-based methods are, in general, sensitive to obstructions, and require the line-of-sight condition. Acoustic-based methods mainly fall into two types: 1) gesture recognition

(classification) [4, 7, 8], which requires training for each gesture used, and 2) interaction tracking, which usually is sensitive to medium variations [21, 23, 30]. Furthermore, the acoustic-based methods are often sensitive to ambient noises in the same frequency range. We study vibration-based sensing methods and achieve robust vibration source localization and tracking on different materials through physics informed calibration.

In this paper, we present SurfaceVibe, a surface vibration based approach that tracks interactions (*taps* and *swipes*) through multiple sensors placed on surfaces. To address the challenges to achieve accurate vibration-based tracking despite medium variations, we first study the impulse-like surface waves induced by taps, and design methods that take dispersion and reflection into account to allow accurate Time Difference of Arrival (TDoA) estimation, and hence accurate localization. Then we investigate the body wave induced by friction from the stick-slip motion of the swipe, which we refer as ‘slip pulses’ [1]. We segment the swipe signals into individual slip pulse signals at different locations for segmented TDoA estimation. Finally, multilateration is utilized to obtain locations of the slip pulses. To validate our system, we performed a series of experiments that test the accuracy of locating taps and tracking swipes with various surface/sensing area sizes.

The main contributions of this paper are:

- We present an on-surface human interaction (tap & swipe) tracking system with vibration sensing.
- We study the properties of waves induced by taps and swipes, and develop algorithms in order to achieve accurate interaction tracking on ubiquitous surfaces.
- We characterize and evaluate the system through surfaces of various materials and settings with both taps and swipes.

The rest of the paper is structured as follows: First of all, we present real world use-cases of the system in Section 2. Then, we provide the background knowledge that supports our work in Section 3. Next, we present the system in Section 4. Furthermore, we describe our experiment setup, analyze the TDoA estimation, and discuss the experiment results in Section 5. In addition, we discuss the possible extensions of this work in Section 6 and the prior work that is related to our system in Section 7. Finally, we conclude our work in Section 8.

2 MOTIVATING USE-CASES

A ubiquitous and larger input sensing method allows 1) easy interaction with increasing number of small, low-power IoT devices, 2) extended interaction ability for individuals with limited mobility, such as kids and patients, and 3) convenient ambient input to improve the user experience. We envision the usage of our system in three major ways. 1) fixed sensor location. For vibration sensors already deployed in the environment for structural health monitoring, a specific area could be targeted for interaction. In this case, the system only needs to be calibrated for once if there are no further structural changes. This deployment can be applied in public areas to provide interactive advertisement surface; 2) semi-fixed sensor location. For IoT devices with vibration sensors (smart appliances) that are not moved often, the area covered by a set of devices could be used for interaction. The system then needs calibration every time the devices are moved to compensate for the

structural variance. This deployment can provide an interaction area to control smart appliance in the smart home even with dirty hands; 3) mobile sensor location. Multiple mobile devices could provide a designated input area for instant usage. The system would need calibration every time it is used. This deployment can be used for enabling/improving group gaming experience.

3 BACKGROUND

SurfaceVibe employs interaction-induced vibrations on physical surfaces that travel through the surface and are recorded by sensors to localize and track the interaction points. Therefore, in this section, we introduce the physics behind: 1) interaction induced waves (impulse v.s. slip-pulse waves) and 2) wave propagation in solids. We design our algorithms based on these properties.

3.1 Impulse v.s. Slip-pulse Waves

We study two types of interactions on surfaces, *taps* and *swipes*, which produce different mechanical waves. The former induces surface waves due to impact force while the latter produces body waves due to friction.

Impact-induced vibrations are produced by a single point of contact on surfaces (e.g., taps) [2]. The force applied to a surface causes it to deform. As the contact point is relieved of the force, the surface retracts due to its elasticity. This elasticity generates surface waves propagating outward from the point of contact, similar to ripples generated in water when a stone is dropped [2].

Friction-induced vibrations are observed when two objects slide against each other (e.g., fingers swiping against a surface). Stick-slip is a general form of friction that induces vibrations [1, 11]. When an object slides on surfaces, it will ‘stick’ because of static friction and the unevenness of the surface, then the force applied to it causes it to overcome the static friction and slide or ‘slip’ [1, 22]. When these two states are alternating, the friction between the two sliding objects changes between static friction and kinetic friction [22]. Since typically static friction is larger than kinetic friction, such alternating friction causes a sudden jump in the velocity of the movement, resulting in slip pulse [1, 22] along the swipe. These slip pulses induce a wave that travels at an angle in the material as a combination of different types of waves dominated by body wave [1]. In this work, we leverage such slip pulse signals to locate and track the vibrations along the swipe.

3.2 Wave Propagation in Solids

Wave propagation in solid is dispersive in nature, and different frequency components travel at different speeds in the range of 50 to 300 m/s [14, 21, 26]. Therefore, when the wave travels through the solid, the dispersion introduces distortion into the vibration signal, making vibration-based localization a challenge [14].

Different waves have different attenuation models. An impact-induced vibration (tap) is dominated by surface waves (Rayleigh waves, spreading $\propto 1/r^{1/2}$) [25, 26]. On the other hand, a friction-induced vibration (swipe) is dominated by body waves (shear wave, spreading $\propto 1/r$) [25, 32]. Using these wave propagation characteristics, we infer that the friction-induced vibrations decay faster than impulse-induced vibrations and thus have less reflection on edges.

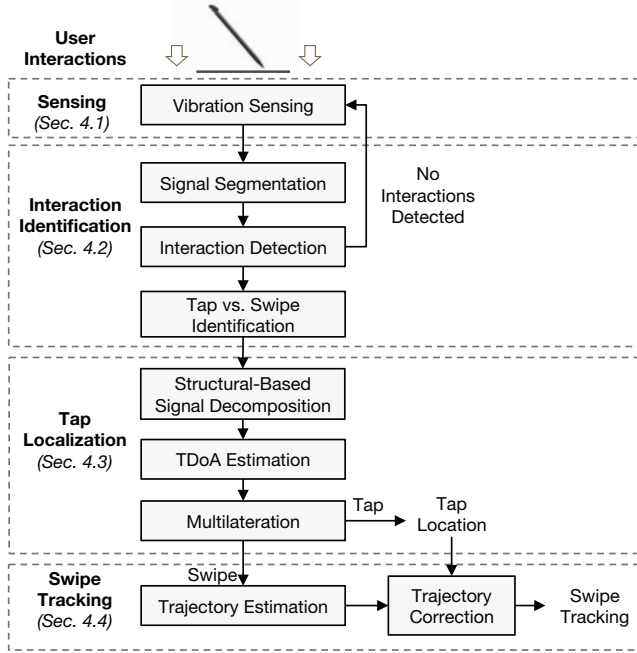


Figure 1: SurfaceVibe System Overview.

4 SYSTEM

SurfaceVibe is a vibration-based sensing system that tracks interactions on common surfaces. It infers the point of impact for taps and trajectory for swipes from vibration induced by user interactions on a surface. The system consists of four modules as shown in Figure 1: 1) sensing, 2) interaction identification, 3) tap localization, and 4) swipe tracking.

4.1 Sensing

The sensing module obtains interaction induced vibrations with sensors placed on the target surface. Geophones (SM-24) [9] detect vibrations caused by surface particles moving perpendicular to the target surface. They are low-cost vibration sensors that are sensitive to waves investigated here¹. The signals are then amplified before digitization using an oscilloscope. Figure 2 (a) shows a raw signal collected by the system.

4.2 Interaction Identification

Once the raw signal is obtained, the interaction induced vibration signal needs to be extracted and each tap or swipe needs to be identified. 1) First, the signal is segmented by sliding windows. 2) Then the segments induced by interactions are distinguished from ambient noise. These consecutively detected segments make interaction events. 3) Finally, the system identifies the interaction events as taps or swipes.

Signal Segmentation. The raw vibration signal is segmented into small windows to conduct interaction detection. For each

¹The retail price in U.S. is around 60 dollar [9], and similar products are available at a price of less than 1 dollar in China [27]. The prototype of the entire system costs \$250 with only sensors and op-amps. We estimate the commercial scale production can lower this price to \$30, including processing units and sensors.

segmented signal, the signal energy is calculated and sent to the interaction detection. The segment length is selected to cover a long enough duration to allow accurate cross-correlation based TDoA estimation, which will be further explained later in Section 5.1.3.

Interaction Detection. The interaction detection is conducted through anomaly detection [17]. To do so, a Gaussian noise model (mean μ and standard deviation σ) is calculated by the signal segments of noise signals. Then, when an investigated segment's signal energy is beyond the value of $\mu + 3\sigma$, the segment is detected as an interaction segment. The consecutive windows, which are detected as anomalies, make an interaction event.

Tap v.s. Swipe Identification. The tap signal is an impulse-like signal with fast decay and short duration, while the swipe signal often lasts over seconds with continuous high signal energy after the initial impulse. Figure 2 (a) shows an example of a swipe from 0.4s to 2.4s, with an initial tap at 0.3s. The system identifies an event to be a swipe if the segments above the threshold last over one second. The system identifies the interaction and conducts different algorithms based on the type of signal detected: If it is a tap, the system conducts tap localization (Section 4.3). If a swipe is detected after the initial tap, the system conducts tap localization (Section 4.3) on the initial tap and then tracks the rest of the friction induced vibration (Section 4.4).

4.3 Tap Localization

The tap localization module obtains the location of taps. Before using the system, a calibration (Section 4.3.1) to extract the surface/structural characteristics through taps on designated points is conducted. When the system is in action, it first decomposes the signal based on the structural characteristics (Section 4.3.2). Then the system calculates the pairwise Time Difference of Arrival (TDoA) on the extracted signal components (Section 4.3.3). Finally, the multilateration is applied on the extracted TDoA to obtain the location of the signal (Section 4.3.4).

4.3.1 Calibration. Different materials respond to the interaction differently, inducing vibrations with different frequency components and propagation velocities. Therefore, finding the frequency band that minimizes dispersion effects in the designated sensing area allows the system to achieve accurate TDoA estimation. Furthermore, obtaining the propagation velocity is important for converting TDoA to absolute locations. Thus, a calibration phase is needed to determine these two values for different surfaces.

SurfaceVibe utilizes a few taps at designated locations (between each sensor pair) as calibration inputs. The system scans through the wavelet scales and finds the scale that gives correct relative locations of the taps. The system then scans through wave propagation velocity values, and calculates the localization error for calibration points. The wave propagation in solids is within a range of 50 to 300 m/s [26], and the calibrated velocity in our evaluation falls within this range.

Finally, the system selects the velocity that minimizes the sum of the localization errors for all designated calibration points. We apply the selected wave propagation velocity on both the taps and the swipe slip pulses, since the slip pulse signals have complicated wave components. We use the calibration velocity as a representation of the velocity for a specific surface.

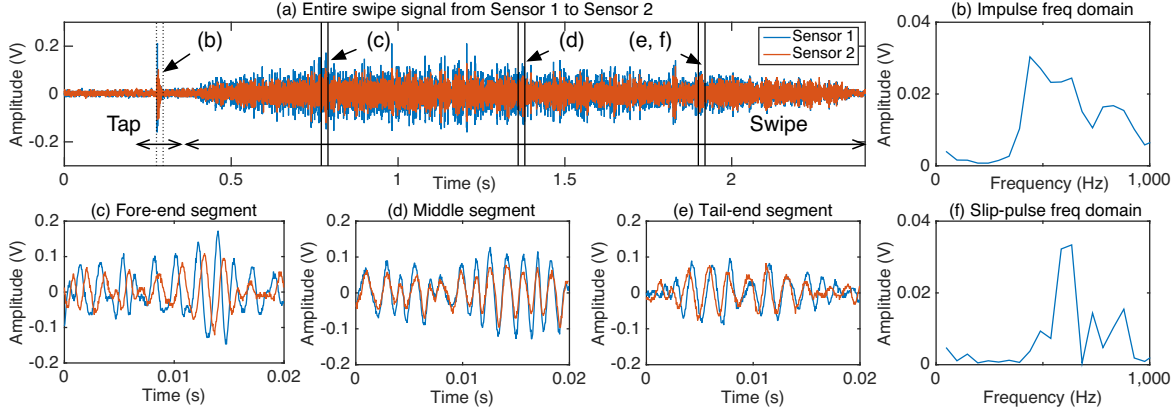


Figure 2: Tap and swipe signal TDoA progression. A swipe occurs from Sensor 1 to Sensor 2. (a) shows the swipe signals detected by these sensors respectively. (b) shows the frequency domain of the initial tap as the finger first makes contact with the surface. (c, d, e) show the signal segments marked out by black lines. (f) shows the frequency domain of the slip-pulse shown in (e). Signals in (c) demonstrate a shift where the blue line is leading in time of arrival, meaning the signal source is closer to Sensor 1. In (d), the red line and blue line have similar phase. (e) shows that in the end part of the signal, the shift is reversed as that shown in (c).

4.3.2 Structure-Based Signal Decomposition. For impulse-like signals like taps, wavelet-based decomposition is effective for band selection and filtering [14]. The detected taps are first decomposed using continuous wavelet transform. Then they are reconstructed on the frequency band selected in the calibration phase. The selection of the band determines the robustness of the TDoA estimation on the specific surface area, which will be discussed in tap evaluation section later.

4.3.3 TDoA Estimation. To localize and track the interaction based on event signals, SurfaceVibe calculates the Time Difference of Arrival (TDoA) of event signals detected at different sensors. Various TDoA estimation methods have been explored for different deployment details [14, 24]. We selected the first peak of arrival since the first peak is less likely to be impacted by reflections [21].

4.3.4 Multilateration. Localization is then performed to estimate where on the surface an input event occurred to induce the investigated signals. This is primarily achieved by using multilateration with the pairwise TDoA values from different sensors. Multilateration is a common technique used to determine the location of a source by comparing the TDoA of signals with different distance towards different sensors [12]. For a pair of sensors, the difference in distances between them results in a hyperbolic curve with an infinite number of locations that satisfy the measurements. When there are multiple hyperbolic curves from different pairs of sensors, the location of their intersection is considered as the source location [14]. The Levenberg Marquardt algorithm [13] is used to find the solution of this intersection as a least squares curve-fitting problem. In addition, since there is noise in the TDoA estimation, the calculated location may fall out of the defined sensing area boundaries. SurfaceVibe checks the boundary conditions and discards those out of bounds as invalid detections.

4.4 Swipe Tracking

The swipe tracking module outputs the estimated trajectory of a given swipe signal. A complete swipe signal often consists of two parts: 1) the initial contact part, which is an impulse-like signal, and 2) the stick-and-slip part, which can be considered as consecutive slip pulses. The localization of the initial contact part has been discussed in Section 4.3. In this section, we will focus on 1) the usage of the slip pulse of the friction induced vibration to localize each signal segment within a swipe, and 2) the intuition of using the initial tap's location to correct the trajectory estimation.

4.4.1 Trajectory Estimation. The swipe tracking module keeps localizing consecutive signal segments within a swipe and forms a trajectory. Figure 2 (a) shows an example of a swipe signal detected by two synchronized sensors. Figure 2 (c, d, e) show three segments selected at the fore-end, middle, and tail-end part of the signal marked out in Figure 2 (a) with black lines.

Unlike taps, slip pulses show more concentrated frequency components than impulses, as shown in Figure 2 (b, f). This is caused by the higher attenuation rate of the body wave, so that when the wave arrives the sensor, some frequencies already die down, leaving fewer frequency components, hinting at lower dispersion. In addition, the reflection may also be lower than that of taps due to the higher attenuation rate. With less dispersion and reflection, correlation is visible between segments from different sensors without the need for wavelet analysis as shown in Figure 2 (c, d, e).

SurfaceVibe thus extracts TDoA using cross-correlation from multiple consecutive segments within a swipe and localizes each of them. Their locations make the trajectory of the swipe, which is capable of describing arbitrary movements. Similar to the tap localization, we check the condition of the estimated location and discard those out of boundary or of low confidence (low cross-correlation peak value) segments as invalid.

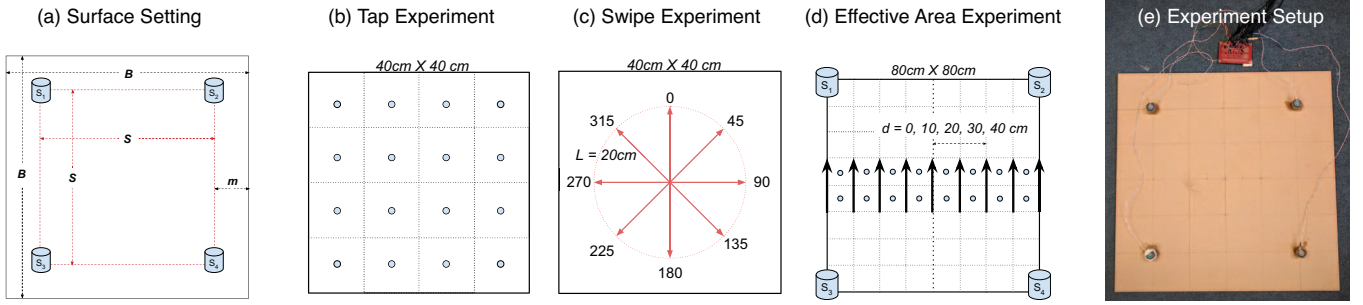


Figure 3: Experiment setup. Dots and arrows indicate tap location and swipe length/direction respectively. (a) shows the surface setting, B is the size of the board, S is the size of the sensing area, defined as distance between sensors, m is the margin from sensing area to board edges. We evaluate different B and S combination with interactions shown in (b, c) within a $40\text{cm} \times 40\text{cm}$ interaction area. (d) shows the effective area experiment setting with a $80\text{cm} \times 80\text{cm}$ interaction area. (e) shows an example experiment setup on the baseline board ($B = 61\text{cm}$, $S = 40\text{cm}$).

We mainly focus on linear swipes in this paper for evaluation purposes. SurfaceVibe first calculates the direction of the swipe by conducting a linear fit on the detected locations of the time windows and determining the heading based on the time window sequence. Then, it determines the distance traveled based on the two farthest points projected on the fitted line. In this way, SurfaceVibe is able to estimate the trajectory of a swipe.

4.4.2 Trajectory Correction with Initial Tap. Once the swipe tracking module estimates the trajectory, it confirms the results using the location estimated with the initial tap. While dispersion is less of a concern with swipes than with taps, it can still impact the TDoA estimation. However, the wavelet filter is effective in removing dispersion effects with impulse-like signals, which could be applied on the initial tap of the swipe. Therefore, the estimated location of the initial tap could be used to further correct the tracking estimation. However, due to the variance of the human motion, some of the initial taps are weak and confused with noise, resulting in a falsely detected initial tap signal and wrong location estimation.

Therefore, the system combines the two techniques and only relies on the initial tap as the correction when the estimated trajectory and tap agree with each other. We define ‘agree’ as: the initial tap location 1) is closer to the beginning of the swipe than the end, and 2) has a distance to the fitted line of the swipe less than a threshold (in our case 1 cm). The system combines the initial tap and the swipe by taking the initial tap location into account and re-estimating the direction and length of the swipe with this extra point.

5 EVALUATION

To understand the system performance, we conduct experiments on various surface settings. We first introduce the design of the experiments (Section 5.1). Then we present and analyze the results of tap localization (Section 5.2) and swipe tracking (Section 5.3).

5.1 Experiment Design

In this section, we introduce the experiment design in three aspects: 1) the evaluating metrics, 2) parameters/variables, and 3) the experimental setup.

5.1.1 Metrics. The metrics are selected to evaluate the tap localization and swipe tracking estimation error. For each metric, we evaluate both error and precision. The error and precision of taps and swipes are different, therefore we define them separately in this section.

Tap Error. Tap error is measured by the localization error, which is the distance between the estimated location and the ground truth location. The precision is measured by the scattering radius of the estimated location with the same ground truth location.

Swipe Error. Swipe error is measured by the length and angle error of the estimated trajectory compared to the ground truth trajectory since we investigate linear trajectory swipes. The length error is positive when the estimation length is longer than that of ground truth, and negative when shorter. The clockwise angle errors are considered as positive values, and the counter-clockwise errors as negative values. Because of this, the standard deviation (referred as std for short in later sections) of the error would be effective to describe the system performance here since the average could be canceling out. The precision indicates the accuracy of the tracking in following the trajectory. It is measured by the distance between the estimated location of each segment and the trajectory. In the following sections, we refer to it as trajectory error.

5.1.2 Parameters. We investigated four major parameters to demonstrate the robustness of the system under different scenarios: the surface material, the surface size, distance between sensors, and effectiveness of different sensing areas on the board.

Surface Material. Different surface materials have different dispersion/reflection conditions and wave propagation velocities. To further understand the system robustness and limitations under different materials, we evaluate the system by comparing the tap and swipe errors in these scenarios. Five different surface materials are investigated, including wood, iron, cement, stone, and ceramic. These surfaces were chosen as a representation of materials and surfaces found in a person’s everyday life, such as tables, cabinets, and walls. For the first four materials, we find samples of size $61\text{cm} \times 61\text{cm}$, therefore we set $B = 61\text{cm}$, $S = 40\text{cm}$ shown in Figure 3 (a) as the baseline. The ceramic surface sample used here is $41\text{cm} \times 41\text{cm}$ as it is the only size available.

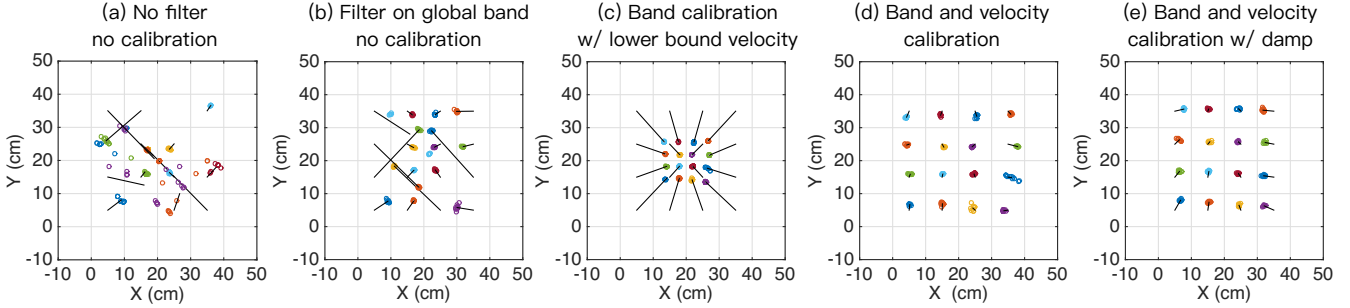


Figure 4: Tap localization examples. Each tap location has 10 data points plotted in one color, they form a cluster and a line is drawn from the center of the cluster to the ground truth location.

Margin Size. Different surface sizes may cause different reflection effects when the margin between the sensor and the board edge changes. In our experiment, we first set the specific sensor deployment setting (the board margin size m) $m = 1\text{ cm}$ as shown in Figure 3 (a). Next, we vary the m , from 1 cm to 30 cm , with incremental of 10 cm (board size B is increased by 20 cm). The experiment is done on wood surfaces only, since wood can be cut into these sizes.

Distance between Sensors. Different distances between sensors indicate different wave travel distances, which determine the signal to noise ratio as well as the dispersion effect for inputs from a designated interaction area. For the largest surface (Figure 3 (a) $B = 101\text{ cm}$) we evaluate the sensing range by change the value S from 40 cm to 80 cm with incremental 10 cm . For each case, the tap and swipes are at the same location as shown in Figure 3 (b, c) within the central $40\text{ cm} \times 40\text{ cm}$ area of the board.

Effective Sensing Area. For large scaled surfaces, the dispersion effects may still show in TDoA estimation. The filtered signal frequency concentrates at a specific band but not a single frequency, meaning the dispersion will be noticeable when the waves travel over longer distances. To evaluate effects on different parts of sensing area, we tap and swipe at locations shown in Figure 3 (d) on a surface of $B = 101\text{ cm}$, $S = 80\text{ cm}$.

5.1.3 Experimental Setup. We conducted the experiments in a room with enough space to place the largest surface investigated on the floor. For each scenario, the evaluated surface is placed at the same location of the room for consistency. Figure 3 (e) demonstrates the settings for the testing surfaces. Since the sample board is not coupled with the floor like these materials will appear in people's everyday life (e.g., as part of a table/wall), we represented real-world table/wall conditions by placing sand-filled weights ($20\text{ cm} \times 5\text{ cm} \times 2\text{ cm}$) around the sensing area in some experiments to enhance the coupling and damp the wave reflection at the loose edges. The geophones are placed on the surfaces with bee's wax to preserve the high-frequency signals [14] for experimental purposes. The data is collected with an oscilloscope at a sampling rate of 25 kHz to provide 1 cm resolution for up to 250 m/s waves (Section 3.2) when used to estimate TDoA. We control the swipe speed with a metronome at a speed of 10 cm/s . The segment window size is 0.02 s to cover a 0.2 cm distance, which is small enough to realize the resolution limitation of the system. The experiments for each

parameter set involve two parts: tap (Section 5.2) and swipe (Section 5.3). Calibration (Section 4.3.2) was conducted before each scenario was carried out. We use a pen to tap and swipe for consistency. In addition, we include swipes using a fingernail in Section 5.3.1. The number of incidences for each scenario investigated is 10.

5.2 Evaluation I: Tap Localization

Tap localization is achieved by studying properties of the impulse-induced surface wave and utilizing a wavelet filter to reduce the dispersion effects. To evaluate the localization algorithm, we compare error rates when different methods are applied. Furthermore, we evaluate the effects of filtering and calibration.

5.2.1 Tap: Dispersion & Calibration. The challenge faced by localization of impulse-like signals through the surface vibration lies in dispersion of wave propagation. Figure 4 shows an example of tap localization results when the dispersion is handled through different methods. Figure 4 (a) shows the localization with raw signal and using cross correlation to obtain TDoA estimation (the same as applied on the swipe segments). The four locations near the center show higher accuracy and precision than the rest. This is because the noise and dispersion make the TDoA estimation unstable when the tap point is far away from the board center.

Wavelet-based signal decomposition allows the system to localize taps at the same location with high precision. Figure 4 (b) shows the localization with signal filtered on a *global band* (417 Hz , median wavelet scale for all materials). However, the results still exhibit variable accuracy, indicating that the error is caused by the surface responding of specific frequency.

The selection of the frequency band to be extracted from the decomposed signal is the key to achieve high accuracy in addition to high precision. Figure 4 (c) shows the localization with signal filtered on a band (625 Hz) selected through calibration discussed in Section 4.3.2 and with a *lower bound velocity* (60 m/s , the minimum velocity used for calibration to ensure points fall into the boundaries) used in calibration. Although the estimated locations are skewed inward towards the center due to the underestimated propagation velocity, the relative locations of the taps are correct compare to those in Figure 4 (b).

Next, we show the results when both filtering band and wave velocity are selected from our calibration method in Figure 4 (d). The accuracy of the estimated location shows less than 3 cm error

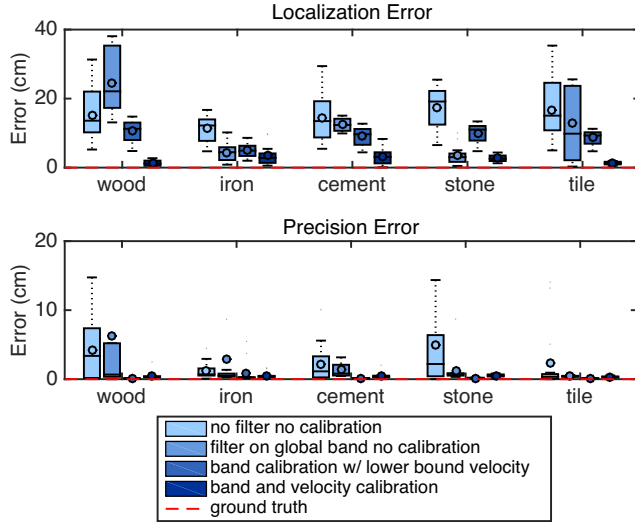


Figure 5: Tap localization results on different materials. When there is no filter and no calibration, the error rate is high for all materials. The global band filter and the velocity calibration improve the accuracy, and when both applied, the system achieves 6X lower error rate through all tested materials.

and high precision. We further investigated the case where the surface has damped edges, meaning the reflection is reduced, as shown in Figure 4 (e). Since the TDoA estimation for tap is based on the first peak of the signal, the reflection reduction does not significantly affect the result. Therefore, in the next section, we focus on the comparison of the first four scenarios through different materials.

5.2.2 Tap: Surface Material. Figure 5 shows box plots² of tap localization results on different materials. To understand the importance of band selection for different materials, we selected the global band as discussed in the last section to apply on all the materials, and the results are shown in Figure 5. We observe that different materials exhibit variable performances on the global band: iron and stone achieve low error rate, while the rest have a high error rate. To understand the importance of velocity selection, we compare applying the calibrated band on each material and applying a lower bound velocity in the range of Rayleigh wave on all the materials. The localization error for lower bound velocity is higher than that of selected velocity due to the consistent inward/outward skew shown in Figure 4 (c).

The estimations utilizing calibration on both filtering band and velocity have consistently lower errors than other cases, with an average localization error reduction of 2.4 cm from 8.6 cm (only calibrate filter band), 9.8 cm (filter on a global band), and 14.8 cm (no filter), with 3.5X, 4X, and 6X decrease in error rate respectively. In addition, when filtered on the selected band, the precision error is lower than 0.5 cm, as compared to the 2.4 cm when filtering on

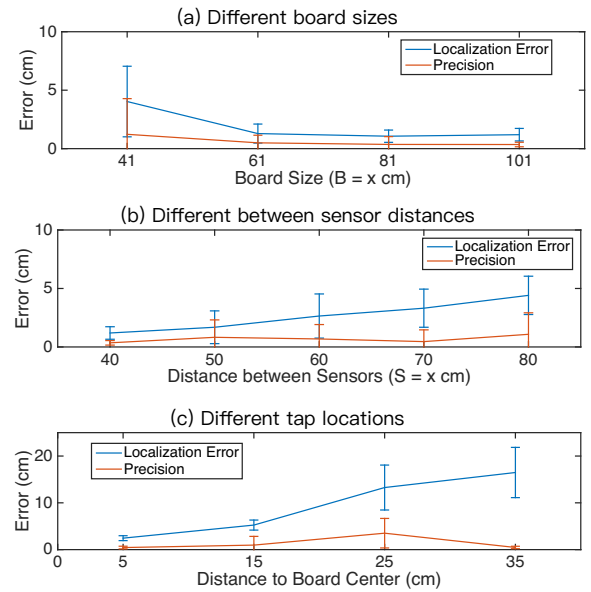


Figure 6: Tap localization results on (a) different board sizes, (b) different between sensor distances, and (c) different tap locations. In general, settings with larger distance to edge and smaller sensing area achieve lower error rate due to less reflection and dispersion.

global band and 2.9 cm when no filter is applied. The results show that with the properly selected filtering band and wave velocity, the system achieves up to 6X lower localization error.

5.2.3 Tap: Margin Size. For the same size of sensing area ($S = 40$ cm), different margin sizes including $m = 10, 20, 30$ cm shows similar level of localization error (respectively 1.3, 1.1, and 1.2 cm) as shown in Figure 6 (a)³. For size $m = 1$ cm, the localization error is up to 4 cm. The size of the sensing area in this case is almost the same size as the board. As a result, the sensors are placed right at the corners of the board, where the boundary conditions could be more complicated. Furthermore, the smaller board resides less stable as taps are applied, resulting in higher noise and error.

5.2.4 Tap: Distance between Sensors. For the same size of interaction area and same size of the surface, the difference in distance to sensing area also affects the sensing ability of the system. We investigate this factor by the surface setting of $B = 101$ cm, $S = 40, 50, 60, 70, 80$ cm. Figure 6 (b) shows the errors of localization and precision respectively. When the distance between the sensors and the sensing area increases, the average localization errors goes up from 1.2 cm to 4.4 cm. This is because of the fact that as the interaction area increases the calibrated velocity (average velocity for the entire board) is no longer well suited due to the heterogeneity of the plywood material. That is also why the localization error increases while the precision error stays at a similar level.

²A box plot shows the mean (circle), median (middle line), quartiles (rectangle box), fences (outside box line), and outliers (cross markers) of the data points.

³A line plot shows the mean (line point) and standard deviation (error bar) of the data points.

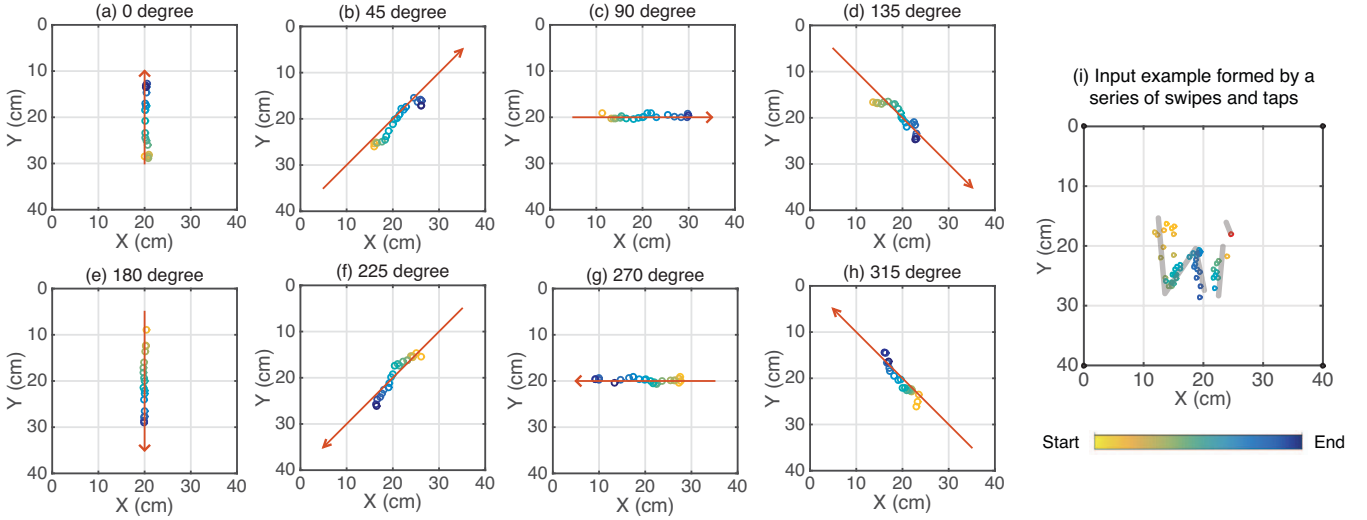


Figure 7: Swipe examples. Swipes are decomposed into a series of localized points as detected by the algorithm. In (a-h), the expected directions and locations are noted by the red arrow. In (i) an input ‘hi’ is formed by a series of swipes and taps.

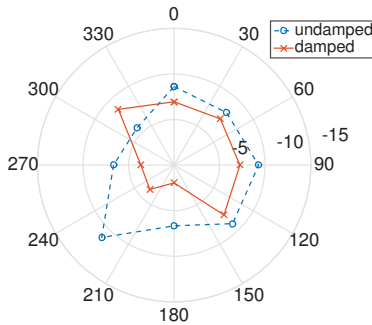


Figure 8: Baseline average length estimation error in eight directions. Damped surface outperforms the undamped surface in seven directions.

5.2.5 Tap: Effective Sensing Area. For the largest sensing area setting $B = 101\text{cm}$, we further investigated the error rate for taps at the different distance towards the center when the sensors are farthest from each other ($S = 80\text{cm}$). Figure 6 (c) shows that the further the points are away from the center, the higher the localization errors are. When the distance of the tap is within 20 cm range from the center, the average localization error is 5.1 cm, while the taps outside this range have up to 18.4 cm average localization error. The precision error values are lower than 5 cm for all testing points. The increase of the localization error is caused by attenuation and dispersion, where the first peak decays to the noise level and cannot be detected.

5.3 Evaluation II: Swipe Tracking

The swipes are tested through surfaces of different materials and settings. We evaluate different surfaces by comparing the parameters

listed in Section 5.1.2. The system demonstrates robust interaction tracking through different parameter sets.

5.3.1 Swipe: Baseline Performance. In the baseline scenario, we mainly evaluate two factors: 1) swipe direction, and 2) swipe instruments with the baseline algorithm. We use wood as the baseline material since further experiments with different sizes are enabled by its easy-to-cut property. We choose $B = 61\text{cm}$ as the baseline size since most (3 out of 4) of the other materials are available in this size.

We evaluate SurfaceVibe with linear swipes to quantify the performance. Figure 7 (a-h) shows an example set of swipes detected by the system towards eight designated directions plotted in Figure 3 (c) on the baseline surface. Arbitrary gestures can be approximated by a series of linear swipes and taps as shown in Figure 7 (i).

The swipe signal can be considered as a sequence of slip pulses, therefore if the reflection of preceding stick-slip signal does not die down after bouncing back at the edge, it will interfere with the later signal, and when a board is well mounted this is less likely. To prevent the reflection, we damp the edges of the investigated surfaces with sand-filled weights placed between edges and the sensing area, so that the wave energy dissipates into the weights before reaching to the edge. The damped surface outperforms the

avg/std	pen cap	fingernail	metal bar
LE (cm)	-4/3.3	-5.6/4.6	-4.1/4.9
AE (degree)	-2/21	-6.7/34	0.55/36
TE (cm)	0.35/0.13	0.36/0.16	0.43/0.15

Table 1: Swipe instrument variance on damped baseline board: average and standard deviation of Length Error (LE), Angle Error (AE), and Trajectory Error (TE) show the similar level of accuracy when different instruments are used.

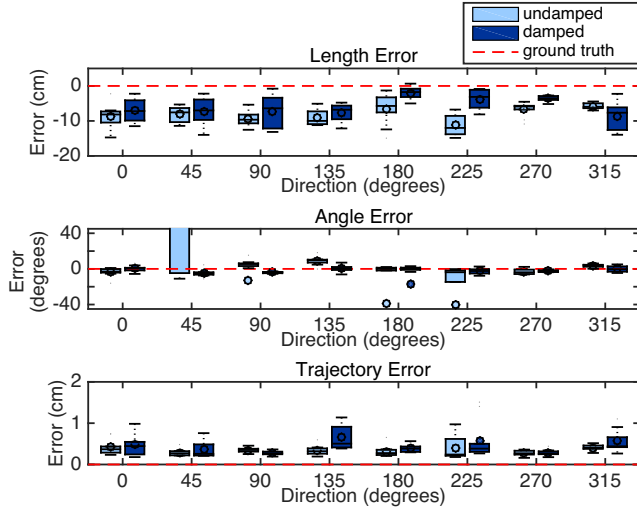


Figure 9: Swipe baseline evaluation. The eight directions demonstrated similar error rate. Angle error has high variation at 45 degrees due to outliers (opposite direction).

undamped one in seven directions in average length estimation as shown in Figure 8. Figure 9 further compares tracking errors when the surface is undamped/damped. The damped surface achieves a lower average length error (-5.8 cm) than the undamped surface (-8.2 cm). The average angle errors in both cases are similar (damped -2 degree, undamped -3.7 degree), but the std of the angle error of the damped surface is 21 degree, $3X$ less than that of the undamped one. The high error rate is caused by outliers for 45 degree undamped surface. Other than that, the eight directions showed similar error rate in Figure 9.

We further conducted experiments on the damped setting with different instruments types including pen, fingernail, and metal bar. These swipe instruments are selected to represent medium, light and heavy swipes respectively. The tracking results are shown in Table 1. These three instruments demonstrated the similar level of error on all three metrics. The pen performs the best out of three, possibly because it is easy to hold and swipe consistently. In the rest of the swipe evaluation, we used the pen to perform all the swipes due to its consistency.

5.3.2 Swipe: Surface Material. Different surface materials have different decay rates and reflection effects. Figure 10 demonstrates the swipe accuracy for five investigated surface materials under four different processing scenarios: 1) undamped surface with baseline algorithm, 2) damped surface with baseline algorithm, 3) undamped surface with initial point correction, and 4) damped surface with initial point correction.

From the comparison in Figure 10, we observe that for wood, iron, cement, and stone, the damped surface achieves a lower error rate of length and angle. The average length estimation error over five materials is -8.7 cm for damped cases and -10.3 cm for undamped cases. Similarly, the average angle error over five materials is -7.16 degree with std of 59.3 degree for damped cases, and -12.8 degree with std of 91.6 degree for undamped cases. The ceramic shows

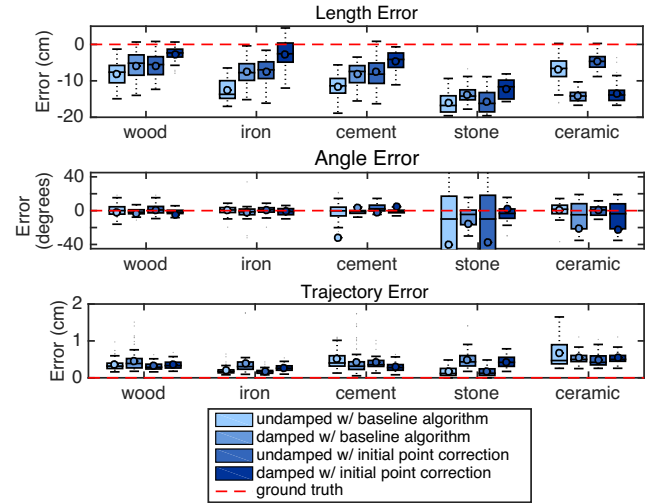


Figure 10: Swipe material evaluation. Five materials are evaluated through four processing methods. Our method shows highest error rate for first four materials, and both damping and using initial tap location allow the system to achieve higher accuracy comparing to baseline. The ceramic shows opposite trends for damped/undamped comparison, which is caused by smaller size (only size available) and the damp is applied within the sensing area.

a different trend on length estimation when the damped surface is used. This could be caused by the different size of the ceramic sample due to the manufacturing limitation. Hence if we compare the first four materials, the damping reduced the average length error from -11.1 cm to -6.9 cm, and the average angle error from -15.5 degree with std of 96 to -2 degree with std of 39 degree ($7X$ reduction, $2X$ reduction). We then further compare the scenarios where the initial tap localization is utilized v.s. those only rely on the estimation of the trajectory. The initial tap location scenarios achieved less length error in all cases, and in average the length error reduced from -10.5 cm to -8.1 cm. The average angle error reduced from -11.2 cm to -8.5 cm. While the trajectory error does not show a clear trend through different scenarios, it does have an average of less than 0.5 cm in all cases.

When the damp and initial tap trajectory correction were both applied, the average length error over five materials reduced from -11.3 cm to -7.2 cm ($1.5X$), and the average angle error reduced from -14.6 degree with std 91 to -6.39 degree with std 61 degree ($2X$). When comparing only the first four materials, this reduction is more clear from -12.2 cm to -4.6 cm ($3X$) and 97 degree to 37 degree ($2.5X$) for average length error and standard deviation of angle errors, respectively. Therefore, both the damping and the trajectory correction contribute to reducing the length and angle error. When both are applied, the system achieves the lowest error rate. This demonstrates SurfaceVibe's robustness when tracking on surfaces of various materials.

5.3.3 Swipe: Margin Size. Figure 11 demonstrates the results of four different sizes of wood boards with damped surfaces. When

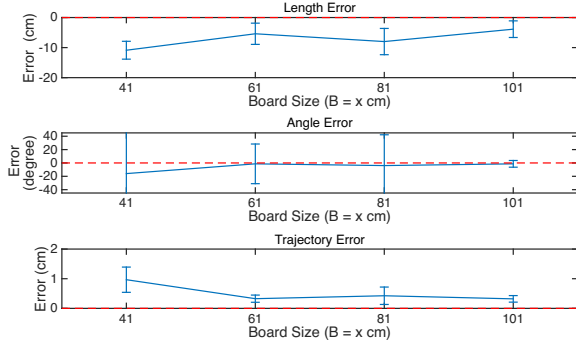


Figure 11: Swipe surface size evaluation. When the surface size increases, i.e., margin between sensor and board edge increases, the error rate decreases, which is caused by the decrease of the reflection detected at the sensors.

the board size is similar to the sensing area, the sensors are right at the corner of the board; hence experiencing the highest reflection effect. The average length error for the surface of $m = 1$ cm is -11 cm, while when m increases to 30 cm by 10 cm intervals, the error is reduced to -5.4 , -8 , and -3.9 cm respectively. Similarly, the average angle error for the surface of $m = 1$ cm is -16 degrees with std 101 degrees, but when m increases, the error std decreases to 30 , 46 , and 5 degree. We can observe a trend that when the margin between the board and the sensing area increases, the swipe error decreases, which we believe is due to the reduction of the reflection waves. When the surface size increases with the sensing area size remaining the same, it means that the distance between the board edge and the sensing area is increasing, which allows the reflection to die down before overlapping with the succeeding waves at the sensors.

5.3.4 Swipe: Distance between Sensors. The distance between sensors on large scaled surfaces will affect the attenuation rate of the interaction signal, as well as dispersion, since the filtered signal is not a single band sine wave. Figure 12 shows the five distances between sensors that we investigated. We observe that when the distance between sensors is increased, the average length error increases (respectively -5 , -4.7 , -10 , -11 , and -7.6 cm). This trend is similar to the one that we observed in tap, which was caused by the emerging of the dispersion effect when the travel distance between the signal source and the sensor increases. The angle error std raises up to 35 degree when the distance between sensors are 50 and 70 cm. As we discussed with the tap evaluation, this change in angle error is due to the heterogeneity of the plywood surface.

5.3.5 Swipe: Effective Sensing Area. This experiment was conducted on the largest surface as described in Figure 3 (d). Swipes that are at different distances from the center were conducted and the swipe tracking results are shown in Figure 13. The average angle error is 11 degrees with std of 42.6 degrees. The length error and the trajectory error increased when the distance between the swipe and center was increased. The average length error for the center swipe (distance to board center is 0 cm) is -5 cm, while the rest are varying between -10 to -12 cm. Similarly, the angle

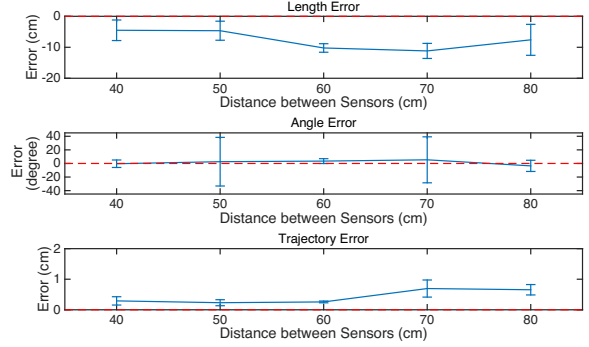


Figure 12: Swipe with different between-sensor distances. When between-sensor distances increase, the error rates increase. This is caused by dispersion effects, which are more severe when waves travel a longer distance to sensors.

error std increased tremendously from less than 1 degree to over 25 degrees when the swipes are moved away from the center due to more severe dispersion as discussed in the tap evaluations.

6 DISCUSSION

In this section, we explore the topics that further discuss the system robustness and possible extension from this paper based on the observations and conclusions we made from the evaluation section.

6.1 System Robustness

The tap and swipe demonstrated in the paper can form arbitrary interactions like a mouse in the designated area. We evaluated surfaces with different materials and sizes that can be found commonly in people's life, and our system demonstrates robust performance through investigated scenarios (Section 5.3.2). Further evaluation could be done on various of surface shapes and heterogeneous materials.

6.2 Sensor Density.

In general, the higher sensor density yields to higher tracking accuracy. The scenario in the paper is targeting at using four sensors to cover an area of from $40\text{cm} \times 40\text{cm}$ to $100\text{cm} \times 100\text{cm}$, which can be used for general input area that a person's arm can extend to. This paper mainly focused on the four-sensor setting on the sensing area of limited sizes. As we observed, larger sensing areas may lead to higher tracking error (Section 5.3.4). Therefore, the density of the sensors can be increased to cover larger sensing area. Furthermore, the application can select the optimal combination of the sensing area v.s. designated accuracy range.

6.3 Edge Reflection & Surface Mounting.

The wave reflection has a large impact on vibration based sensing methods as discussed in Section 5.3. In this paper, we utilized sand weights to reduce the wave reflection at edges, to simulate the following scenarios in real-world settings: 1) the surface is tightly mounted to a solid, such as kitchen counter top; and 2) the target surface area is surrounded by dissipating weights, such as books on a table. The tighter the surface is mounted, the higher the swipe

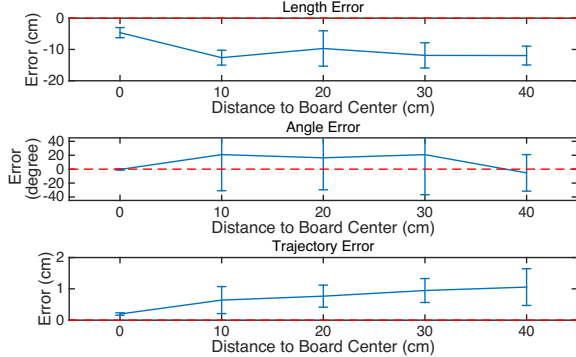


Figure 13: Swipe to board center distance evaluation. The further the interaction from the board center the more severe the dispersion effect. This is because the distances difference between sensors are increased, causing the waves to propagate longer distances.

tracking accuracy will be (Section 5.3.2). As for extreme cases: 1) ground-coupled/wall-coupled surfaces that are tightly attached to a stable entity, and 2) loose surfaces like tables with thin legs, we expect the former to show higher accuracy and the later may show lower accuracy than the results demonstrated in the evaluation section. To make the system more robust to different reflection conditions (e.g., fixed end v.s. free end) [5], further physical insights and how to utilize them to reduce the reflection effects can be explored.

6.4 Multi-point Touch.

In this paper, we discussed the system performance when only one interacting point is on the surface at a time. When multi-point swipes/taps happen on a surface, the vibration signal from different sources will mix together. When the mixed signal is obtained by multiple sensors, we can consider the dispersion effects and the wave properties learned from one pointer interaction and further conduct signal source separation. On the other hand, when multiple impulses occur within the same sensing area, the randomness of the human behavior might cause the onset of the impulses to stagger from each other and hence allow localization and tracking of different impulses [18].

7 RELATED WORK

The key contributions of this work concentrate on two aspects: 1) present an accurate interaction tracking sensing method, and 2) demonstrates the related work in inferring vibration source information through taking physics knowledge into account. Therefore, our related work section focuses on these two aspects.

7.1 Sensing Methods

The existing sensing methods to obtain human interaction on a surface mainly fall into the following categories: the vision-, acoustic-, and vibro-acoustic-based systems.

7.1.1 Vision-Based Systems. Vision-based systems fall into two categories: infrastructural-based and mobile-based design. The

infrastructural based systems often use fixed cameras to capture interfaces [29]. On the other hand, the mobile-based design utilizes air (intangible) [15] and body parts (tangible) [16] as interaction screens. In general, the vision-based methods are prone to the obstruction between the gesture and the camera (e.g., body, hand, arm hair, etc.), hence they may experience more deployments restrictions. SurfaceVibe, in comparison, can be deployed on tabletops/walls with less mounting restrictions.

7.1.2 Acoustic-Based Classification Systems. Others have explored the topic of distinguishing different gestures' locations and shapes through classification methods [4, 7, 8]. These works show the possibility of recognizing and localizing the gestures based on the interaction induced sounds. However, these works focus only on classification-based methods to achieve these results. This means that these systems need a large amount of training data and can only handle gestures that exist in the training database. Our system doesn't need gesture training to track taps and swipes, therefore allowing for more flexible gesture detection and localization.

7.1.3 Acoustic-based Tracking Systems. Other work has adopted acoustic signals to achieve the interaction localization goal. The TDoA and multilateration are used to localize the taps [21, 23, 30]. However, their evaluation experiments are either only done on a specific material or lack of comparison with the ground truth interaction trace. From the shown results, we can observe that the dispersion causes high deviation in localization results. In comparison, our work reduces the dispersion by addressing the nature of impulse and slip pulse waves, thus enabling the vibration-based approach on multiple less ideal materials. We are the first to utilize the wave properties to achieve accurate interaction tracking.

7.2 Vibration Source Tracking and Characterization

In this paper, we demonstrated that utilizing physics information can assist our system in achieving robust vibration source tracking through different materials. Works have been done on robust vibration source tracking and characterization using physical principles, despite limited sensing data/labeling and human involvement. Jia et. al. utilize bed vibration to estimate human heart rate by analyzing the wave propagation model [10]. Han et. al. measure the vibration of the vehicles to estimate their relative location (whether on the same lane) utilizing the physics insight of the vehicle vibration and road conditions [6]. Xu et. al. use structural vibration to infer traffic condition in the street [31]. Furthermore, our prior works on the structural vibration for human information inferring are also the inspiration of this paper [14, 17–20].

8 CONCLUSION

In this paper, we presented SurfaceVibe, a vibration-based sensing technique that turns common surfaces in life into touchpads. We study properties of waves induced by different interactions and utilize these properties to reduce effects of dispersion and to enable accurate localization of taps and swipes. We further characterize different surface materials and settings to evaluate the accuracy and robustness of the system. For impulse-like signals (taps), our filter and calibration method achieves 6X improvements in localization

error. For stick-slip signals (swipe), our algorithm achieves 3X improvement in length estimation error. This system can enable ubiquitous input methods for arbitrary gesture input on surfaces of the future smart home.

ACKNOWLEDGEMENTS

This work is partially supported by NSF (CNS-1149611), Pennsylvania Infrastructure Technology Alliance (PITA), Intel, and Google.

REFERENCES

- [1] GG Adams. 2000. Radiation of body waves induced by the sliding of an elastic half-space against a rigid surface. *Journal of applied mechanics* 67, 1 (2000), 1–5.
- [2] Hugo Bachmann and Walter Ammann. 1987. *Vibrations in structures: induced by man and machines*. Vol. 3. Iabse, Zurich, Switzerland.
- [3] Janie Chang. 2011. Two Extremes of Touch Interaction. <http://research.microsoft.com/en-us/news/features/touch-101711.aspx> (2011). Accessed: 2016-04-10.
- [4] Mayank Goel, Brendan Lee, Md Tanvir Islam Aumi, Shwetak Patel, Gaetano Borriello, Stacie Hibino, and Bi Begole. 2014. SurfaceLink: using inertial and acoustic sensing to enable multi-device interaction on a surface. In *Proceedings of the 32nd annual ACM conference on Human factors in computing systems*. ACM, New York, NY, USA, 1387–1396.
- [5] RD Gregory and I Gladwell. 1983. The reflection of a symmetric Rayleigh-Lamb wave at the fixed or free edge of a plate. *Journal of Elasticity* 13, 2 (1983), 185–206.
- [6] Jun Han, Madhumitha Harishankar, Xiao Wang, Albert Jin Chung, and Patrick Tague. 2017. Convoy: Physical Context Verification for Vehicle Platoon Admission. In *18th International Workshop on Mobile Computing Systems and Applications (HotMobile)*. ACM, Sonoma California, to appear.
- [7] Chris Harrison and Scott E Hudson. 2008. Scratch input: creating large, inexpensive, unpowered and mobile finger input surfaces. In *Proceedings of the 21st annual ACM symposium on User interface software and technology*. ACM, New York, NY, USA, 205–208.
- [8] Chris Harrison, Julia Schwarz, and Scott E Hudson. 2011. TapSense: enhancing finger interaction on touch surfaces. In *Proceedings of the 24th annual ACM symposium on User interface software and technology*. ACM, Santa Barbara, California, 627–636.
- [9] Input/Output Inc. 2006. Geophone SM-24. <https://www.sparkfun.com/products/11744>. (2006). Accessed: 2017-01-24.
- [10] Zhenhua Jia, Musaab Alaziz, Xiang Chi, Richard E Howard, Yanyong Zhang, Pei Zhang, Wade Trappe, Anand Sivasubramaniam, and Ning An. 2016. HB-phone: a bed-mounted geophone-based heartbeat monitoring system. In *Information Processing in Sensor Networks (IPSN), 2016 15th ACM/IEEE International Conference on*. IEEE, Vienna, Austria, 1–12.
- [11] RI Leine, DH Van Campen, A De Kraker, and L Van Den Steen. 1998. Stick-slip vibrations induced by alternate friction models. *Nonlinear dynamics* 16, 1 (1998), 41–54.
- [12] Atri Mandal, Cristina V Lopes, Tony Givargis, Amir Haghhighat, Raja Jurdak, and Pierre Baldi. 2005. Beep: 3D indoor positioning using audible sound. In *Consumer communications and networking conference, 2005. CCNC. 2005 Second IEEE*. IEEE, Las Vegas, NV, USA, 348–353.
- [13] Donald W Marquardt. 1963. An algorithm for least-squares estimation of nonlinear parameters. *Journal of the society for Industrial and Applied Mathematics* 11, 2 (1963), 431–441.
- [14] Mostafa Mirshekari, Shijia Pan, Pei Zhang, and Hae Young Noh. 2016. Characterizing wave propagation to improve indoor step-level person localization using floor vibration. In *SPIE Smart Structures and Materials+ Nondestructive Evaluation and Health Monitoring*. International Society for Optics and Photonics, Las Vegas, NV, USA, 980305–980305.
- [15] Pranav Mistry and Pattie Maes. 2009. SixthSense: a wearable gestural interface. In *ACM SIGGRAPH ASIA 2009 Sketches*. ACM, Yokohama, Japan, 11.
- [16] Takehiro Niikura, Yoshihiro Watanabe, and Masatoshi Ishikawa. 2014. Anywhere Surface Touch: Utilizing Any Surface As an Input Area. In *Proceedings of the 5th Augmented Human International Conference (AH '14)*. ACM, New York, NY, USA, Article 39, 8 pages. DOI : <http://dx.doi.org/10.1145/2582051.2582090>
- [17] Shijia Pan, Amelie Bonde, Jie Jing, Lin Zhang, Pei Zhang, and Hae Young Noh. 2014. Boes: building occupancy estimation system using sparse ambient vibration monitoring. In *SPIE Smart Structures and Materials+ Nondestructive Evaluation and Health Monitoring*. International Society for Optics and Photonics, San Diego, CA, USA, 906110–906110.
- [18] Shijia Pan, Kent Lyons, Mostafa Mirshekari, Hae Young Noh, and Pei Zhang. 2016. Multiple Pedestrian Tracking through Ambient Structural Vibration Sensing: Poster Abstract. In *Proceedings of the 14th ACM Conference on Embedded Network Sensor Systems CD-ROM*. ACM, Stanford, California, 366–367.
- [19] Shijia Pan, Mostafa Mirshekari, Pei Zhang, and Hae Young Noh. 2016. Occupant traffic estimation through structural vibration sensing. In *SPIE Smart Structures and Materials+ Nondestructive Evaluation and Health Monitoring*. International Society for Optics and Photonics, Las Vegas, NV, 980306–980306.
- [20] Shijia Pan, Ningning Wang, Yuqin Qian, Irem Velibeyoglu, Hae Young Noh, and Pei Zhang. 2015. Indoor person identification through footstep induced structural vibration. In *Proceedings of the 16th International Workshop on Mobile Computing Systems and Applications*. ACM, Santa Fe, NM, 81–86.
- [21] Joseph A. Paradiso and Che King Leo. 2005. Tracking and characterizing knocks atop large interactive displays. *Sensor Review* 25, 2 (2005), 134–143. DOI : <http://dx.doi.org/10.1108/02602280510585727> arXiv:<http://dx.doi.org/10.1108/02602280510585727>
- [22] Bo Persson. 2013. *Sliding friction: physical principles and applications*. Springer Science & Business Media, Berlin.
- [23] Duc Truong Pham, Ze Ji, Ming Yang, Zuobin Wang, and Mostafa Al-Kutubi. 2007. A novel human-computer interface based on passive acoustic localisation. In *International Conference on Human-Computer Interaction*. Springer, Beijing, China, 901–909.
- [24] Zheng Sun, Aweek Purohit, Kaifei Chen, Shijia Pan, Trevor Pering, and Pei Zhang. 2011. PANDAA: physical arrangement detection of networked devices through ambient-sound awareness. In *Proceedings of the 13th international conference on Ubiquitous computing*. ACM, Beijing, China, 425–434.
- [25] HP Verhas. 1979. Prediction of the propagation of train-induced ground vibration. *Journal of Sound and Vibration* 66, 3 (1979), 371–376.
- [26] Igor Aleksandrovich Viktorov. 1970. *Rayleigh and Lamb waves: physical theory and applications*. Plenum press, Berlin, Germany.
- [27] Weihai grand exploration instrument co. ltd 2013. Geophone GD-28. <https://world.taobao.com/item/18954260795.htm?fromSite=main&spm=a1z3o.7695460.0.0.31P2hg>. (2013). Accessed: 2017-01-24.
- [28] Jacob O Wobbrock, Meredith Ringel Morris, and Andrew D Wilson. 2009. User-defined gestures for surface computing. In *Proceedings of the SIGCHI Conference on Human Factors in Computing Systems*. ACM, Boston, Massachusetts, USA, 1083–1092.
- [29] Robert Xiao, Chris Harrison, and Scott E. Hudson. 2013. WorldKit: Rapid and Easy Creation of Ad-hoc Interactive Applications on Everyday Surfaces. In *Proceedings of the SIGCHI Conference on Human Factors in Computing Systems (CHI '13)*. ACM, New York, NY, USA, 879–888. DOI : <http://dx.doi.org/10.1145/2470654.2466113>
- [30] Robert Xiao, Greg Lew, James Marsanico, Divya Hariharan, Scott Hudson, and Chris Harrison. 2014. Toffee: Enabling Ad Hoc, Around-device Interaction with Acoustic Time-of-arrival Correlation. In *Proceedings of the 16th International Conference on Human-computer Interaction with Mobile Devices & Services (MobileHCI '14)*. ACM, New York, NY, USA, 67–76. DOI : <http://dx.doi.org/10.1145/2628363.2628383>
- [31] Susu Xu, Lin Zhang, Pei Zhang, and Hae Young Noh. 2016. An Indirect Traffic Monitoring Approach Using Building Vibration Sensing System: Poster Abstract. In *Proceedings of the 14th ACM Conference on Embedded Network Sensor Systems CD-ROM*. ACM, Stanford, CA, 374–375.
- [32] Vladislav A Yastrebov. 2016. Sliding without slipping under Coulomb friction: opening waves and inversion of frictional force. *Tribology Letters* 62, 1 (2016), 1–8.